SCIENTIFIC REPORTS
nature research

OPEN

# Scribble co-operatively binds multiple $\alpha_{1D}$-adrenergic receptor C-terminal PDZ ligands

Received: 4 July 2019
Accepted: 17 September 2019
Published online: 01 October 2019

Eric M. Janezic[1], Dorathy-Ann Harris[1], Diana Dinh[1], Kyung-Soon Lee[1], Aaron Stewart[1], Thomas R. Hinds[1], Peter L. Hsu[1,2], Ning Zheng[1,2] & Chris Hague[1]

**Many G protein-coupled receptors (GPCRs) are organized as dynamic macromolecular complexes in human cells. Unraveling the structural determinants of unique GPCR complexes may identify unique protein:protein interfaces to be exploited for drug development. We previously reported $\alpha_{1D}$-adrenergic receptors ($\alpha_{1D}$-ARs) – key regulators of cardiovascular and central nervous system function – form homodimeric, modular PDZ protein complexes with cell-type specificity. Towards mapping $\alpha_{1D}$-AR complex architecture, biolayer interferometry (BLI) revealed the $\alpha_{1D}$-AR C-terminal PDZ ligand selectively binds the PDZ protein scribble (SCRIB) with >8x higher affinity than known interactors syntrophin, CASK and DLG1. Complementary *in situ* and *in vitro* assays revealed SCRIB PDZ domains 1 and 4 to be high affinity $\alpha_{1D}$-AR PDZ ligand interaction sites. SNAP-GST pull-down assays demonstrate SCRIB binds multiple $\alpha_{1D}$-AR PDZ ligands via a co-operative mechanism. Structure-function analyses pinpoint R1110$^{PDZ4}$ as a unique, critical residue dictating SCRIB:$\alpha_{1D}$-AR binding specificity. The crystal structure of SCRIB PDZ4 R1110G predicts spatial shifts in the SCRIB PDZ4 carboxylate binding loop dictate $\alpha_{1D}$-AR binding specificity. Thus, the findings herein identify SCRIB PDZ domains 1 and 4 as high affinity $\alpha_{1D}$-AR interaction sites, and potential drug targets to treat diseases associated with aberrant $\alpha_{1D}$-AR signaling.**

G protein-coupled receptors (GPCRs) account for ~4% of the human genome and are targets for ~30% of FDA approved drugs[1]. Typically these medications compete with endogenous ligands for orthosteric binding sites, hindering drug selectivity due to the similarity of binding pockets amongst closely related GPCRs. Thus, there is great interest in identifying novel sites to modulate GPCR signaling. To this end, a growing body of research has focused on identifying and characterizing the functional roles of GPCR interacting proteins. Two prominent examples are the β-arrestins[2]; and PDZ (PSD95/Dlg/ZO-1) domain containing proteins, which typically interact with C-terminal PDZ ligands[3,4]. Since the discovery that rhodopsin interacts with inaD[5] and $\beta_2$-adrenergic receptor (AR) with NHERF[6], significant effort has been put forth to understand GPCR:PDZ protein interactions and their potential as drug targets[7–11]. For example, pharmacological disruption of the nNOS:NOS1AP:PSD95:NMDAR protein complex provides an alternative approach to NMDAR antagonists for treating neuropathic pain[12–14] and neuronal excitotoxicity[15], demonstrating the therapeutic potential of targeting PDZ protein interactions to selectively modulate membrane protein function.

Of the three $\alpha_1$-AR GPCR subtypes ($\alpha_{1A}$, $\alpha_{1B}$, $\alpha_{1D}$) that respond to the endogenous catecholamines epinephrine and norepinephrine, only the $\alpha_{1D}$-AR subtype contains a C-terminal Type I PDZ ligand. Yeast 2-hybrid[16] and tandem-affinity purification/mass spectrometry[17] screens initially revealed the $\alpha_{1D}$-AR PDZ ligand interacts with the syntrophin family of PDZ domain containing proteins. Syntrophins enhance $\alpha_{1D}$-AR function via recruiting the Dystrophin Associated Protein Complex (DAPC) and signaling effectors, α-catulin, liprin and phospholipase-Cβ[18]. Improved proteomic analyses subsequently revealed that, in addition to syntrophins, $\alpha_{1D}$-ARs also interact with the multi-PDZ domain containing protein scribble (SCRIB); and that $\alpha_{1D}$-ARs are expressed as modular homodimers, with one $\alpha_{1D}$-AR protomer bound to SCRIB, the other to syntrophin, in all human cell lines examined to date[19]. Strikingly, the $\alpha_{1D}$-AR:SCRIB:syntrophin complex is highly unique – no other GPCRs containing C-terminal Type I PDZ ligands have been shown to interact with both SCRIB and syntrophins[20]. Without significant expression of necessary PDZ proteins, $\alpha_{1D}$-ARs are retained intracellularly

[1]Department of Pharmacology, School of Medicine, University of Washington, 1959 NE Pacific Street, Seattle, WA, 98195, USA. [2]Howard Hughes Medical Institute, University of Washington, Seattle, WA, 98195, USA. Correspondence and requests for materials should be addressed to C.H. (email: chague@uw.edu)

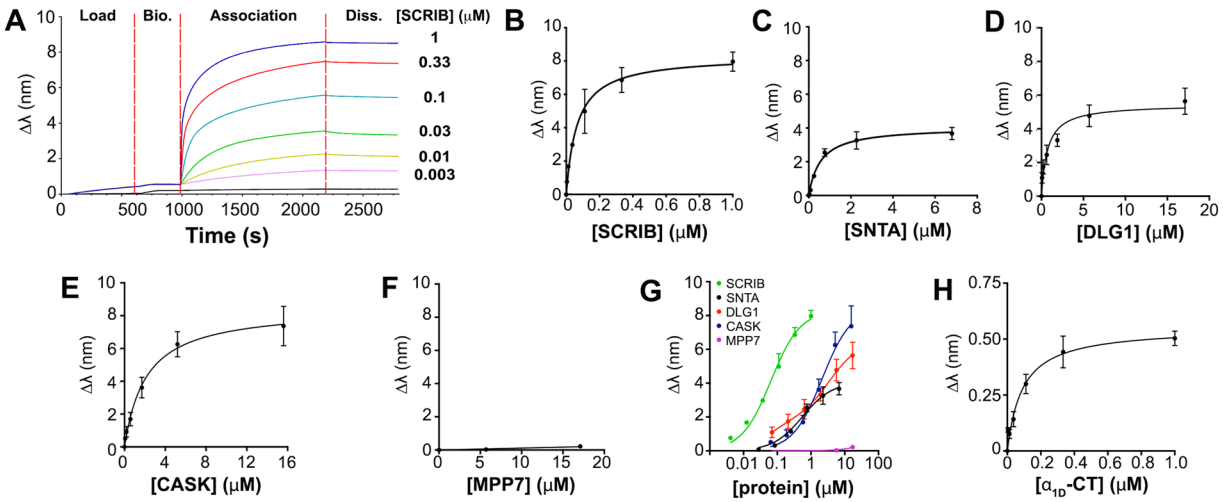


**Figure 1.** *In situ* affinity determination of $\alpha_{1D}$-adrenergic receptor C-terminal PDZ ligand:PDZ protein interactions. (**A**) Real-time biolayer interferometry (BLI) association/dissociation curve measuring binding of $\alpha_{1D}$ C-terminus ($\alpha_{1D}$-CT) to purified scribble (SCRIB). Biotin-labeled $\alpha_{1D}$-CT was immobilized to streptavidin probes. Indicated concentrations of SCRIB were used as analytes. (Bio. = Biocytin, Diss. = Dissociation). (**B**–**F**) Quantified BLI binding data for biotin labeled $\alpha_{1D}$-CT binding to (**B**) SCRIB, (**C**) $\alpha_1$-syntrophin (SNTA), (**D**) human discs large MAGUK scaffold protein 1 (DLG1), (**E**) calcium/calmodulin dependent serine protein kinase (CASK), and (**F**) membrane palmitoylated protein 7 (MPP7). (**G**) Comparative analysis of BLI concentration-response curves for $\alpha_{1D}$-CT:PDZ protein association binding. (**H**) Reverse BLI assay of purified $\alpha_{1D}$-CT (analyte) bound to immobilized biotin-labeled SCRIB (probe). Data are presented as mean ± SEM, n = 3.

and produce weak functional responses[21–23], suggesting this protein:protein interaction site has the potential for pharmacological modulation. Indeed, numerous diseases are associated with aberrant $\alpha_1$-AR function, including hypertension[24], benign prostate hypertrophy[25], bladder obstruction[26], schizophrenia[27], and post-traumatic stress disorder[28,29]. Unfortunately, deleterious side effects (i.e. orthostatic hypotension, reflex tachycardia) are frequently observed with chronic use of non-selective $\alpha_1$-AR antagonists. For example, the doxazosin portion of the ALLHAT anti-hypertensive study was prematurely halted due to increased morbidity[30]. Thus, selectively targeting the $\alpha_{1D}$-AR:SCRIB:syntrophin complex may provide therapeutic benefit, minus the toxicities associated with non-selective $\alpha_1$-AR ligands.

Herein, we employed a combination of biophysical, biochemical and cell-based approaches to acquire structural insights into the $\alpha_{1D}$-AR:PDZ protein complex. Together, our data implicate SCRIB PDZ domains 1 and 4 as the primary anchor sites for the $\alpha_{1D}$-AR. We further highlight differences in $\alpha_{1D}$-AR:PDZ1 versus $\alpha_{1D}$-AR:PDZ4 interactions by identifying unique residues in PDZ4 that are critical for $\alpha_{1D}$-AR binding.

## Results and Discussion

**$\alpha_{1D}$-AR preferentially binds SCRIB PDZ domains 1 and 4.** We previously discovered the $\alpha_{1D}$-AR interacts with multiple PDZ proteins with cell-type specificity: scribble (SCRIB), $\alpha_1$-syntrophin (SNTA), human discs large MAGUK scaffold protein 1 (DLG1), and calcium/calmodulin-dependent serine protein kinase (CASK)[19]. With the goal of elucidating the molecular architecture of this unique, modular GPCR:PDZ protein complex, we employed BioLayer Interferometry (BLI) to quantify equilibrium dissociation constants ($K_D$) for $\alpha_{1D}$-AR PDZ ligand:PDZ protein interactions. cDNAs encoding for the PDZ domains of these proteins were subcloned into a modified pGEX vector (pCOOL), expressed in *E. coli* and purified. Immobilized biotin-labeled peptides containing the distal 20 amino acids of $\alpha_{1D}$-AR ($\alpha_{1D}$-CT) were incubated with purified PDZ proteins and subjected to BLI analysis (Fig. 1A). We first compared $\alpha_{1D}$-CT binding to SCRIB and $\alpha_1$-syntrophin (SNTA), as $\alpha_{1D}$-ARs were found to interact with both PDZ proteins in all human cell lines examined[19]. Remarkably, $\alpha_{1D}$-CT bound SCRIB ($K_D = 70 \pm 20$ nM; Fig. 1B) with ~8 higher affinity than SNTA ($K_D = 0.56 \pm 0.14$ μM; Fig. 1C). DLG1 ($K_D = 0.79 \pm 0.21$ μM; Fig. 1D) and CASK ($K_D = 1.15 \pm 0.21$ μM; Fig. 1E), similar to SNTA, bind $\alpha_{1D}$-CT with lower affinity than SCRIB. MPP7, a known interactor of DLG1 and CASK[31], displayed negligible $\alpha_{1D}$-CT binding (Fig. 1F). The combined rank order of affinity for $\alpha_{1D}$-CT interactions with known PDZ proteins is SCRIB» > SNTA > DLG1 > CASK» > MPP7 (Fig. 1G). $\alpha_{1D}$-CT:SCRIB binding affinity was validated by performing reverse BLI on GST-SCRIB probes incubated in serial dilutions of biotinylated $\alpha_{1D}$-CT ($K_D = 76 \pm 20$ nM; Fig. 1H).

A defining structural characteristic of SCRIB includes the presence of four clustered PDZ domains in the C-terminal portion of the polypeptide. Thus, we questioned if $\alpha_{1D}$-CT selectively associates with targeted PDZ domains on SCRIB. Individual PDZ domains were purified as GST-fusion proteins from *E. coli* and subjected to BLI analysis. SCRIB PDZ1 ($K_D = 1.93 \pm 0.49$ μM; Fig. 2A) and SCRIB PDZ4 ($K_D = 1.14 \pm 0.23$ μM; Fig. 2D) bind $\alpha_{1D}$-CT with the highest affinity, followed by SCRIB PDZ2 ($K_D = 14.9 \pm 5.44$ μM; Fig. 2B) and SCRIB PDZ3 ($K_D = 44.16 \pm 13.52$ μM; Fig. 2C).

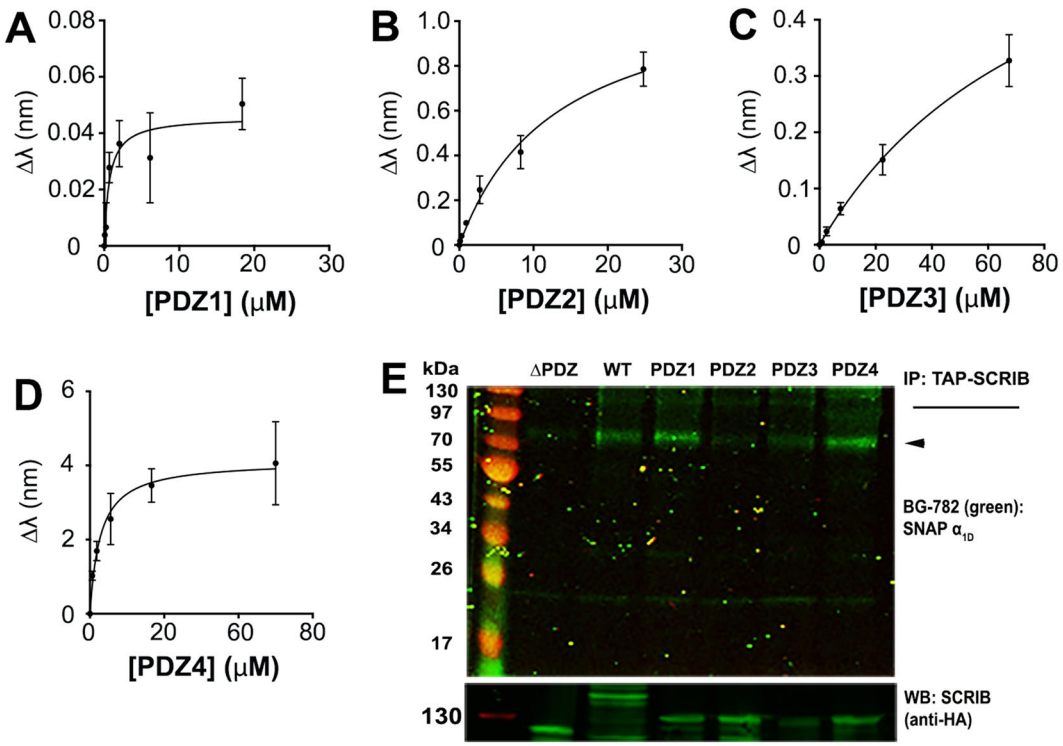


**Figure 2.** *In situ* and *in vitro* analysis of $\alpha_{1D}$-adrenergic receptor C-terminal PDZ ligand:SCRIB single PDZ domain interactions. (**A–D**) Biolayer interferometry (BLI) analyses of immobilized biotin-labeled $\alpha_{1D}$-CT binding to (**A**) SCRIB PDZ domain 1 (PDZ1), (**B**) SCRIB PDZ domain 2 (PDZ2), (**C**) SCRIB PDZ domain 3 (PDZ3) and (**D**) SCRIB PDZ domain 4. BLI data are presented as mean ± SEM, n = 3. (**E**) *Top panel*, PAGE NIR of BG-782 labeled SNAP-$\alpha_{1D}$-AR co-immunoprecipitated with TAP-SCRIB containing all 4 PDZ domains (WT), PDZ domain 1 (PDZ1), 2 (PDZ2), 3 (PDZ3) or 4 (PDZ4), or no PDZ domains (ΔPDZ) from HEK293 cell lysates. *Bottom panel*, Anti-HA western blot of upper gel for listed TAP-SCRIB constructs. ◄ indicates SNAP-$\alpha_{1D}$-AR monomer band.

Next, SCRIB containing all 4 PDZ domains (WT), SCRIB mutants containing single-PDZ domains (PDZ1, PDZ2, PDZ3, PDZ4), and SCRIB lacking all 4 PDZ domains (ΔPDZ) were subcloned into the pGlue vector to add N-terminal tandem affinity purification (TAP) epitope tags. HEK293 cells were transfected with TAP-SCRIB constructs and cell lysates were subjected to immunoblotting to verify expression (Suppl. Fig. 1). Next, constructs were transiently transfected into HEK293 cells stably expressing SNAP-$\alpha_{1D}$-AR. Cell lysates were affinity purified with streptavidin beads. Samples were labeled with BG-782 to detect SNAP-$\alpha_{1D}$-AR and imaged with PAGE NIR. As shown in Fig. 2E, SNAP-$\alpha_{1D}$-AR co-immunoprecipitated robustly with SCRIB WT, PDZ1, PDZ4, and to a lesser extent, with PDZ3. As expected SCRIB ΔPDZ produced no significant SNAP-$\alpha_{1D}$-AR binding. Thus, *in vitro* analysis of $\alpha_{1D}$-AR:SCRIB interactions concurs with prior *in situ* BLI results.

Taken together, these data implicate SCRIB PDZ1 and PDZ4 as the central scaffolds of the $\alpha_{1D}$-AR complex. Based on our discovery that CASK and DLG1 bind with relatively low affinity to the $\alpha_{1D}$-AR PDZ ligand, and that previous studies have reported SCRIB can interact with additional PDZ proteins (reviewed in[32]), we suspect CASK and DLG1 are recruited to the $\alpha_{1D}$-AR complex indirectly by SCRIB. For example, DLG1 can be indirectly recruited to SCRIB via GUKH, which interacts with SCRIB PDZ2 in *Drosophila* synaptic boutons[33], or LGL − a known interactor with both DLG1 and SCRIB[34,35]. Additionally, DLG1, CASK, and LIN-7A are expressed as a tripartite complex *in vitro* and *in vivo*[36–38], suggesting DLG1 may be recruiting CASK and LIN-7A to the $\alpha_{1D}$-AR complex via indirect interactions with SCRIB.

**$\alpha_{1D}$-CT:SCRIB binding is co-operative.** A key finding from BLI studies was the notable difference in $\alpha_{1D}$-CT binding affinity for SCRIB containing all 4 PDZ domains (70 nM) relative to each individual SCRIB PDZ domain (1.14–44.16 μM). The divergent $\alpha_{1D}$-CT:SCRIB binding affinities are suggestive of a co-operative binding mechanism, in that the binding of a single $\alpha_{1D}$-CT PDZ ligand to SCRIB enhances the affinity of subsequent intramolecular $\alpha_{1D}$-CT:SCRIB PDZ binding events. We tested this model by quantifying the affinity of SCRIB C-terminal truncation mutants missing PDZ4 (ΔPDZ4) or PDZ3 and PDZ4 (ΔPDZ34) with BLI. $\alpha_{1D}$-CT bound SCRIB ΔPDZ4 ($K_D = 0.14 \pm 0.02$ μM; Fig. 3A) and SCRIB ΔPDZ34 ($K_D = 0.16 \pm 0.01$ μM; Fig. 3B) with ~2x lower affinity than SCRIB WT (not significant, One-way ANOVA with Tukey's post-hoc test), but ~6x higher affinity than SCRIB PDZ1 ($p = 0.001$, One-way ANOVA with Tukey's post-hoc test) or PDZ4 alone ($p = 0.07$, One-way ANOVA with Tukey's post-hoc test). In the reverse experiment, $\alpha_{1D}$-CT bound SCRIB PDZ3 and PDZ4 (PDZ34) with substantially lower affinity ($K_D = 0.34 \pm 0.09$ μM; Fig. 3C; not significant, One-way ANOVA with Tukey's post-hoc test) than SCRIB WT, but greater than SCRIB PDZ4 (not significant, One-way ANOVA with Tukey's post-hoc test).

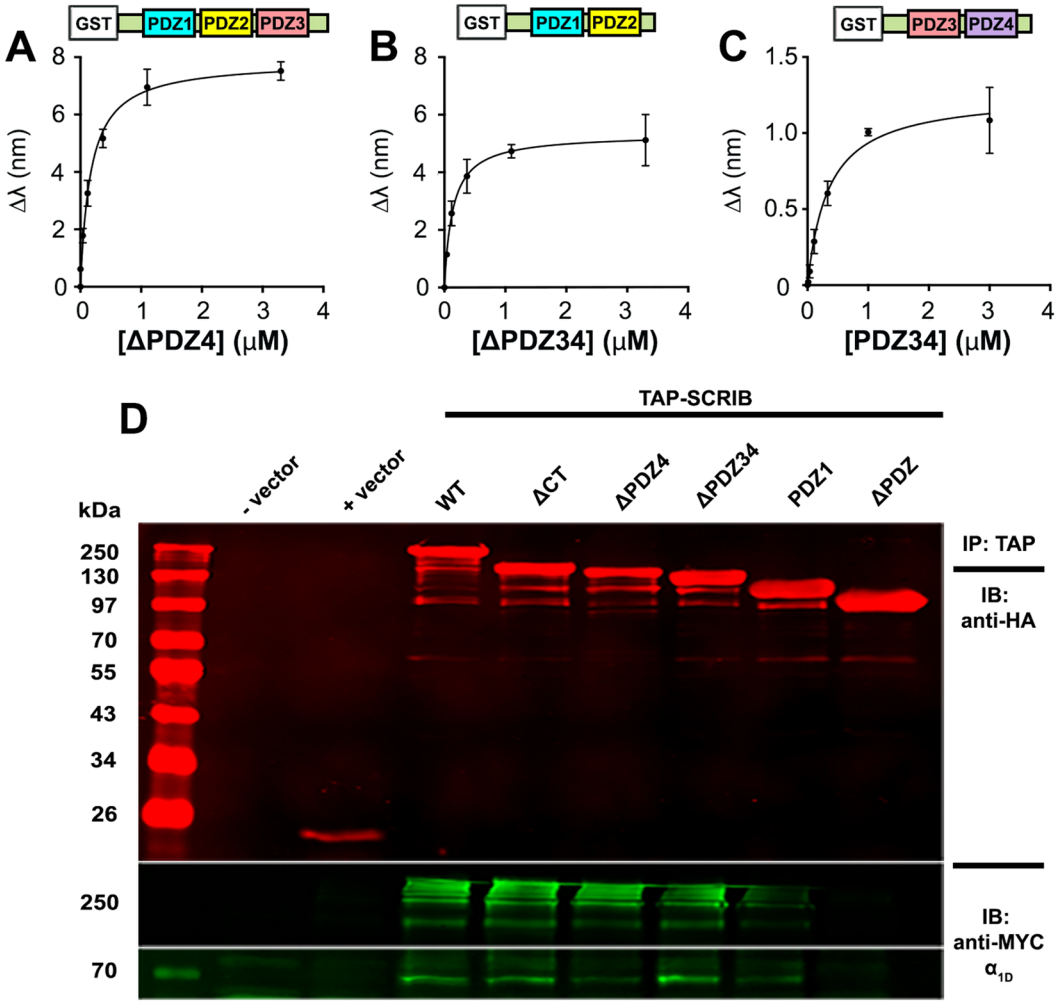


**Figure 3.** *In situ* and *in vitro* analysis of $\alpha_{1D}$-adrenergic receptor C-terminal PDZ ligand:SCRIB truncation mutant interactions. (**A–C**). Biolayer interferometry (BLI) analyses of $\alpha_{1D}$-CT binding to SCRIB ΔPDZ4 (**A**), SCRIB ΔPDZ34 (**B**) and SCRIB PDZ34 (**C**). BLI data are presented as mean ± SEM, n = 3. (**D**) Co-immunoprecipitation of myc-$\alpha_{1D}$-AR with transfection vehicle (− vector), empty pGlue vector (+vector), TAP-SCRIB containing all 4 PDZ domains (WT), or sequentially truncated at the C-terminus (CT), PDZ domain 4 (ΔPDZ4), PDZ domain 3 (ΔPDZ34), PDZ domain 2 (PDZ1) or PDZ domain 1 (ΔPDZ) from HEK293 cell lysates. Shown are western blots of TAP-SCRIB constructs (*top panel*), myc-$\alpha_{1D}$-AR multimers (*middle panel*) and monomers (*bottom* panel). For full blots reference Supplemental Fig. 2.

Thus, these findings are suggestive of a co-operative $\alpha_{1D}$-CT:SCRIB binding modality, and provide additional support for previous studies suggesting SCRIB PDZ34 forms a "supramodule" binding site for PDZ ligands[39].

We then tested the ability of SCRIB truncation mutants to co-immunoprecipitate with full length $\alpha_{1D}$-AR in mammalian cell culture. TAP-SCRIB mutants were co-transfected with myc-$\alpha_{1D}$-AR into HEK293 cells, digitonin-solubilized as cell lysates, immunoprecipitated with streptavidin beads and probed for anti-HA (TAP-SCRIB; Fig. 3D, Suppl. Fig. 2, *top panel*) and anti-myc ($\alpha_{1D}$-AR; Fig. 3D, *lower panels*). As shown, successive C-terminal SCRIB deletions produced progressive decreases in $\alpha_{1D}$-AR monomer (Fig. 3D, *bottom panel*, 68 kDa) and multimer (Fig. 3D, *middle panel*, ~250 kDa) signal, whereas SCRIB ΔPDZ produced no detectable $\alpha_{1D}$-AR interaction. Of note, the most dramatic decrease in $\alpha_{1D}$-AR binding was observed with SCRIB containing only PDZ1 (Fig. 3D, lane PDZ1).

Next, SNAP GST-tag pulldown assays were used to test the proposed co-operative model of $\alpha_{1D}$-AR:SCRIB binding. The experimental approach involved the creation of a novel reporter construct: a SNAP-epitope tag adjacent to the N-terminus of the distal 16 amino acids of the $\alpha_{1D}$-CT (SNAP-$\alpha_{1D}$-CT). PAGE near infrared (NIR) analysis of HEK293 cell lysates transfected with SNAP-$\alpha_{1D}$-CT displayed protein bands of expected size 21.7 kDa (Fig. 4A). Next, GST-SNAP-$\alpha_{1D}$-CT was expressed in and purified from *E. Coli*, then eluted via TEV cleavage (Fig. 4B). SNAP-$\alpha_{1D}$-CT was pre-labeled with 1 μM SNAP-substrate BG-782 and subjected to PAGE NIR/LICOR Odyssey NIR imaging (Fig. 4C) to generate a standard curve (Fig. 4D). Glutathione agarose beads were incubated with previously described GST-SCRIB constructs, mixed with serial dilutions of labeled SNAP-$\alpha_{1D}$-CT, eluted, and analyzed with PAGE NIR. 10 μM BG-782 pre-labeled SNAP-$\alpha_{1D}$-CT was included in each gel as a

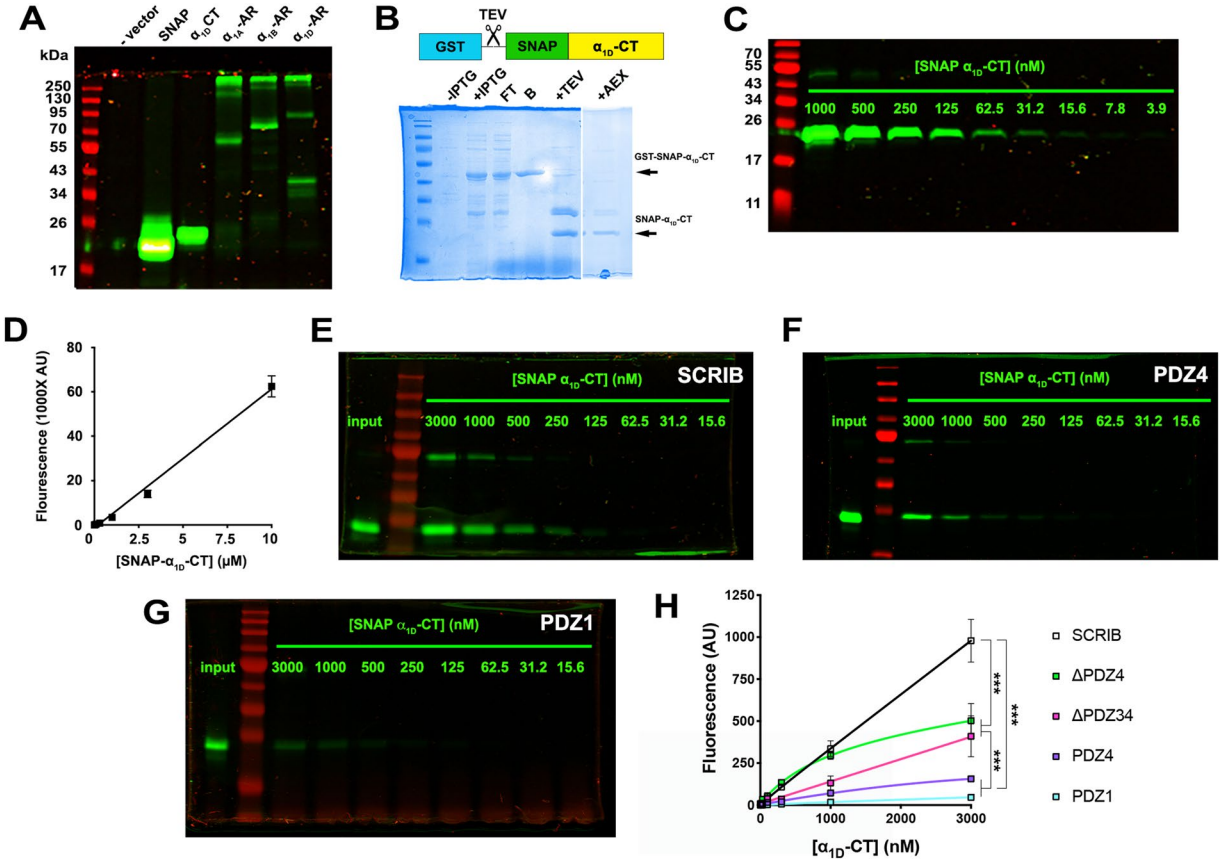


**Figure 4.** SNAP-$\alpha_{1D}$-adrenergic receptor C-terminal PDZ ligand:GST-SCRIB pulldown assays indicate a co-operative binding model. (**A**) PAGE NIR of HEK293 cell lysates transfected with vehicle alone (− vector), pSNAP vector (SNAP), N-terminal SNAP-tagged $\alpha_{1D}$-AR C-terminus ($\alpha_{1D}$-CT), $\alpha_{1A}$, $\alpha_{1B}$ and $\alpha_{1D}$-AR. (**B**) Coomassie stain of GST-SNAP-$\alpha_{1D}$-CT purification ± IPTG induction, unbound (FT), bound to beads (B), following TEV cleavage (+TEV) and anion exchange chromatography (AEX). (**C**) PAGE NIR of purified SNAP-$\alpha_{1D}$-CT pre-labeled with BG-782. (**D**) SNAP-$\alpha_{1D}$-CT standard curve plotting concentration of BG-782 labeled SNAP-$\alpha_{1D}$-CT versus fluorescence quantified at $\lambda = 800$ nm. (**E–G**) Representative PAGE NIR gels of SNAP-$\alpha_{1D}$-CT pulldowns with GST-SCRIB (**E**), GST-PDZ4 (**F**), or GST-PDZ1 (**G**). (**H**) Concentration-response curves quantifying SNAP-$\alpha_{1D}$-CT bound to GST-SCRIB, SCRIB truncated before PDZ domain (ΔPDZ4), before PDZ domain 3 (ΔPDZ34), SCRIB PDZ1, or SCRIB PDZ4 (mean ± SEM, n = 3–4). ***$p < 0.001$, One-way ANOVA with Tukey's post-hoc test.

normalization control (Fig. 4E–G, denoted as INPUT). In accordance with previous BLI experiments, SCRIB WT bound SNAP-$\alpha_{1D}$-CT in a concentration-dependent manner (Fig. 4E), with higher avidity than PDZ4 (Fig. 4F; $p < 0.0001$, One-way ANOVA with Tukey's post-hoc test) or PDZ1 (Fig. 4G; $p < 0.0001$, One-way ANOVA with Tukey's post-hoc test). Interestingly, SCRIB ΔPDZ4 (~48% of SCRIB WT; $p < 0.0001$, One-way ANOVA with Tukey's post-hoc test) and ΔPDZ34 (~34% of SCRIB WT; $p < 0.0001$, One-way ANOVA with Tukey's post-hoc test) produced maximal SNAP-$\alpha_{1D}$-CT binding responses that were less than SCRIB WT, yet greater than single SCRIB PDZ domain constructs (<10% of SCRIB WT, Fig. 4H; $p < 0.0001$, One-way ANOVA with Tukey's post-hoc test). Taken together, our findings support the model that multiple $\alpha_{1D}$-AR CT PDZ ligands bind a single molecule of SCRIB via a co-operative mechanism.

A similar model has been proposed for numerous proteins containing multiple PDZ domains[40–43]. For example, PDZ domains 1 and 2 of PSD-95 exhibit greater affinity for binding partners Kv1.4, NR2B, and CRIPT when expressed in tandem[40]. The PDZ domains of syntenin also work co-operatively to bind syndecan dimers – syntenin PDZ2:syndecan interaction is a pre-requisite for syntenin PDZ1:syndecan binding[41,42]. A recent study similarly found that PDZ domains 2 and 3 of PTPN13 show enhanced binding for the PDZ ligand of APC when expressed together compared to individual domain constructs[43]. These previously characterized interactions further support our findings that the $\alpha_{1D}$-CT:SCRIB interaction is co-operative.

**Structure-function analyses identify R1110$^{PDZ4}$ as a selectivity determinant for $\alpha_{1D}$-CT binding.** We next compared $\alpha_{1D}$-CT:SCRIB binding parameters to previously identified SCRIB PDZ1 and PDZ4 interactors. SCRIB PDZ1 interacts with >20 proteins[32], whereas PDZ4 interacts with NOS1AP[44], APC[45], p22phox[46], NMDA receptor subunits GLUN2A and GluN2B[47], and DLC3[48]. Remarkably, $\alpha_{1D}$-CT has the highest reported affinity to date of all reported SCRIB PDZ4 interactors. For example, the PDZ ligand of p22phox binds SCRIB

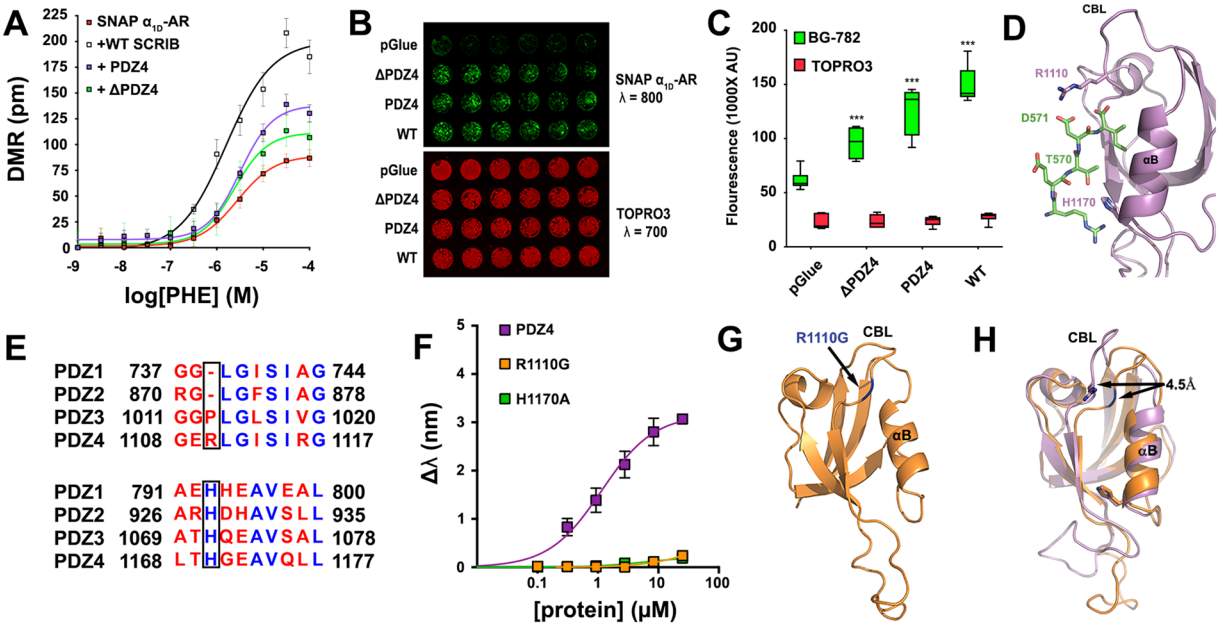


**Figure 5.** Structure-function analysis of the $\alpha_{1D}$-CT:SCRIB PDZ4 interaction. (**A**) Dynamic mass redistribution assays quantifying phenylephrine efficacy in HEK293 cells stably expressing SNAP-$\alpha_{1D}$-AR alone, or transfected with SCRIB WT, PDZ4, or SCRIB containing only PDZ domains 1, 2 and 3 (ΔPDZ4). Data are the mean of 12 replicates ± SEM. (**B**) Cell surface expression of SNAP-$\alpha_{1D}$-AR in HEK293 cells transfected with vector control (pGlue), ΔPDZ4, PDZ4, or SCRIB WT (*top panel, green*); nuclear stain TO-PRO-3 was used to normalize for cell number (*bottom panel, red).* (**C**) Quantification of data from B (mean ± SEM, n = 3, 6 replicates; ***$p < 0.001$ from pGLUE, One-way ANOVA with Tukey's post-hoc tests). (**D**) Molecular docking model of $\alpha_{1D}$-CT:SCRIB PDZ4 interaction (purple = PDZ4, green = $\alpha_{1D}$-CT, PDB ID = 4WYT used for model). (**E**) Sequence alignment of SCRIB PDZ domains (boxes indicate residues identified in **D**). (**F**) Biolayer interferometry (BLI) analysis of SCRIB mutations H1170A and R1110G on $\alpha_{1D}$-CT binding (mean ± SEM, n = 3). (**G**) X-ray crystallography structure of SCRIB PDZ4 R1110G (mutation highlighted in blue; PDB ID = 6EEY). (**H**) R1110G (orange) causes a 4.5 Å shift in carboxylate binding loop, as determined by superposition with WT PDZ4 (purple).

PDZ4 with $K_D = 40\,\mu M$[46], whereas the NMDA receptor PDZ ligands bind SCRIB PDZ4 with $K_D > 150\,\mu M$[47]. Thus, targeting SCRIB PDZ4 may provide the highest opportunity to disrupt $\alpha_{1D}$-AR function without perturbing other SCRIB complexes.

We first investigated the impact of SCRIB PDZ4 on $\alpha_{1D}$-AR functional responses. Label-free dynamic mass redistribution (DMR) signaling assays were performed using HEK293 cells stably expressing SNAP-$\alpha_{1D}$-AR alone or transiently co-expressing SCRIB WT, SCRIB PDZ4 or SCRIB ΔPDZ4. Concentration-response curves were generated for the selective $\alpha_1$-AR agonist phenylephrine to facilitate efficacy comparison between transfection conditions. As shown, phenylephrine efficacy was enhanced by all SCRIB constructs with rank order WT > PDZ4 > ΔPDZ4 > pGLUE vector control (Fig. 5A). Next, the ability of SCRIB mutants to promote $\alpha_{1D}$-AR plasma membrane trafficking were assessed using a 96-well plate near infrared imaging cell surface assay. The rank order of SCRIB constructs for promoting $\alpha_{1D}$-AR plasma membrane trafficking was WT > PDZ4 > ΔPDZ4 > pGlue (Fig. 5B,C). We have previously reported that α-syntrophin interacts with $\alpha_{1D}$-AR in the endoplasmic reticulum[49], and that SCRIB and syntrophin co-localize and compete for the PDZ ligand of $\alpha_{1D}$-CT[19]. Therefore, we propose the $\alpha_{1D}$-AR:SCRIB interaction occurs in the endoplasmic reticulum to facilitate trafficking to the plasma membrane. However, further studies are warranted to determine the precise mechanism and machinery by which this complex formation is regulated.

Functional studies indicate targeting SCRIB PDZ4 alone may be a useful approach to modulate $\alpha_{1D}$-AR processes *in vivo*. However, this requires a thorough understanding of the structural determinants governing selectivity of the $\alpha_{1D}$-CT PDZ ligand for SCRIB PDZ4. Molecular docking that employed the solved crystal structure of SCRIB PDZ4 (PDB ID: 4WYT; refs.[39,50,51]) was used to predict $\alpha_{1D}$-CT:SCRIB PDZ4 interactions. Our model identified $D571^{\alpha 1D\text{-}AR}$:$R1110^{PDZ4}$ of the carboxylate binding loop and $T570^{\alpha 1D\text{-}AR}$:$H1170^{PDZ4}$ of α-helix B as possible $\alpha_{1D}$-CT PDZ ligand interaction sites within SCRIB PDZ4 (Fig. 5D). SCRIB PDZ domain sequence alignment revealed that R1110, but not H1170, is unique to PDZ4, suggesting that this residue may be responsible for the specificity of $\alpha_{1D}$-AR to PDZ4 (Fig. 5E). In support of our structural prediction, purified PDZ4 harboring either R1110G or H1170A mutations ablates $\alpha_{1D}$-CT binding (Fig. 5F).

Previous structural and biophysical studies have identified homologous histidine residues within Type I PDZ domains that control ligand specificity[52–55]. However, the structural role of R1110 is unknown. To resolve the mechanistic underpinnings of this interaction, the crystal structure of PDZ4 R1110G was solved to 1.15 Å resolution (Fig. 5G; Table 1; Suppl. Fig. S3). A superposition of the R1110G mutant with WT PDZ4 reveals a 4.5 Å

| | SCRIB PDZ4 R1110G |
|---|---|
| **Data collection** | |
| Space group | P 1 21 1 |
| Cell dimensions | |
| *a*, *b*, *c* (Å) | 27.29, 40.24, 32.26 |
| α, β, γ (°) | 90, 97.85, 90 |
| Resolution (Å) | 31.96–1.145 (1.186–1.145)* |
| $R_{merge}$ | 0.06674 (0.07563)* |
| $I/\sigma I$ | 12.82 (3.48)* |
| Completeness (%) | 82.58 (3.40)* |
| Redundancy | 4.4 (1.0)* |
| **Refinement** | |
| Resolution (Å) | 31.96–1.145 (1.186–1.145)* |
| No. reflections | 20613 (85)* |
| $R_{work}/R_{free}$ | 0.1571 (0.1385)/0.1818 (0.1574)* |
| No. atoms | 1646 |
| Protein | 692 |
| Ligand/ion | — |
| Water | 131 |
| *B*-factors | |
| Protein | 7.36 |
| Ligand/ion | — |
| Water | 16.20 |
| R.m.s. deviations | |
| Bond lengths (Å) | 0.008 |
| Bond angles (°) | 1.35 |

**Table 1.** Data collection and refinement statistics for Scribble PDZ4 R1110G mutant (molecular replacement). *Values in parentheses are for highest-resolution shell.

shift of the carboxylate binding loop (Fig. 5H). We predict this shift creates steric hindrance that prevents the interaction between $I572^{\alpha 1D\text{-}AR}$ and PDZ4. Previous studies have found PDZ ligand:PDZ domain interactions are dictated by interactions of the C-terminal residue of the PDZ ligand[52,55,56]. For example, *in situ* peptide library screens revealed 89% of peptides interacting with the PDZ domain of nNOS contain a C-terminal valine[56]. Thus, we propose that preventing $I572^{\alpha 1D\text{-}AR}$ from interacting with PDZ4 is sufficient to inhibit $\alpha_{1D}$-CT binding.

Finally, we leveraged the information gathered from our structural studies to understand how mutations in either PDZ1 and/or PDZ4 affect the $\alpha_{1D}$-CT interaction in context of the core binding protein, SCRIB. This involved introducing H793A PDZ1 and H1170A PDZ4 mutations into GST-SCRIB (Fig. 6A, schematic) and subjecting to $\alpha_{1D}$-CT BLI analysis. As shown, SCRIB H1170A retains significant $\alpha_{1D}$-CT binding with affinity ($K_D = 0.32 \pm 0.08\,\mu M$; Fig. 6A) similar to the SCRIB PDZ34 construct (Fig. 3D). Mutating the equivalent amino acid in SCRIB PDZ1, H793A, produced a species that retains $\alpha_{1D}$-CT binding, with ~20x lower affinity ($K_D = 7.34 \pm 4.53\,\mu M$; Fig. 6B) than SCRIB PDZ4 H1170A. Strikingly, introducing both H793A and H1170A mutations into SCRIB abolished $\alpha_{1D}$-CT binding as measured by BLI (Fig. 6C).

## Conclusions

The present study strongly suggests that $\alpha_{1D}$-CT is capable of binding each SCRIB PDZ domain, but preferentially interacts with SCRIB PDZ1 and PDZ4. Also, the $\alpha_{1D}$-CT:SCRIB interaction appears to be co-operative, potentially driving multiple $\alpha_{1D}$-AR PDZ ligands to bind one molecule of SCRIB. We previously reported $\alpha_{1D}$-ARs can be expressed as modular homodimers in human cells, with one $\alpha_{1D}$-AR protomer bound to SCRIB, the other to syntrophin and the DAPC[19]. Based on the results of the present study, it is possible that $\alpha_{1D}$-AR homodimers interact simultaneously with both SCRIB PDZ1 and PDZ4, with at least one $\alpha_{1D}$-AR protomer interacting with the syntrophin:DAPC via the non-SCRIB bound PDZ ligand, and the other bound to a second syntrophin:DAPC module, or the DLG:CASK:LIN-7A tripartite complex (36–38; hypothetical schematic of $\alpha_{1D}$-AR:SCRIB:DAPC shown in Fig. 6D). Alternatively, an $\alpha_{1D}$-AR protomer may bind another SCRIB, anchoring interconnected $\alpha_{1D}$-AR:SCRIB:DAPC complexes at the plasma membrane in human cells. Finally, we demonstrate that SCRIB $R1110^{PDZ4}$ serves as a unique $\alpha_{1D}$-CT interface site that could be targeted to modulate $\alpha_{1D}$-AR pharmacodynamics.

## Methods

**Plasmids and chemicals.** Molecular cloning was performed using inFusion HD cloning technology (Clontech/Takara Biotech, Mountain View, CA). Constructs used for bacterial expression were sub-cloned into a modified pGEX vector to add GST-tags. For mammalian expression, constructs were inserted into pGLUE to add streptavidin binding protein/TEV/calmodulin binding protein tags; or pSNAPf to add SNAP-epitope tags; or pcDNA3.1 to fuse MYC tags. BG-782 SNAP substrate was from New England Biolabs (Ipswich, MA). PageRuler Prestained NIR Protein Ladder was used for all PAGE NIR (Thermo Fisher Scientific, Waltham, MA).

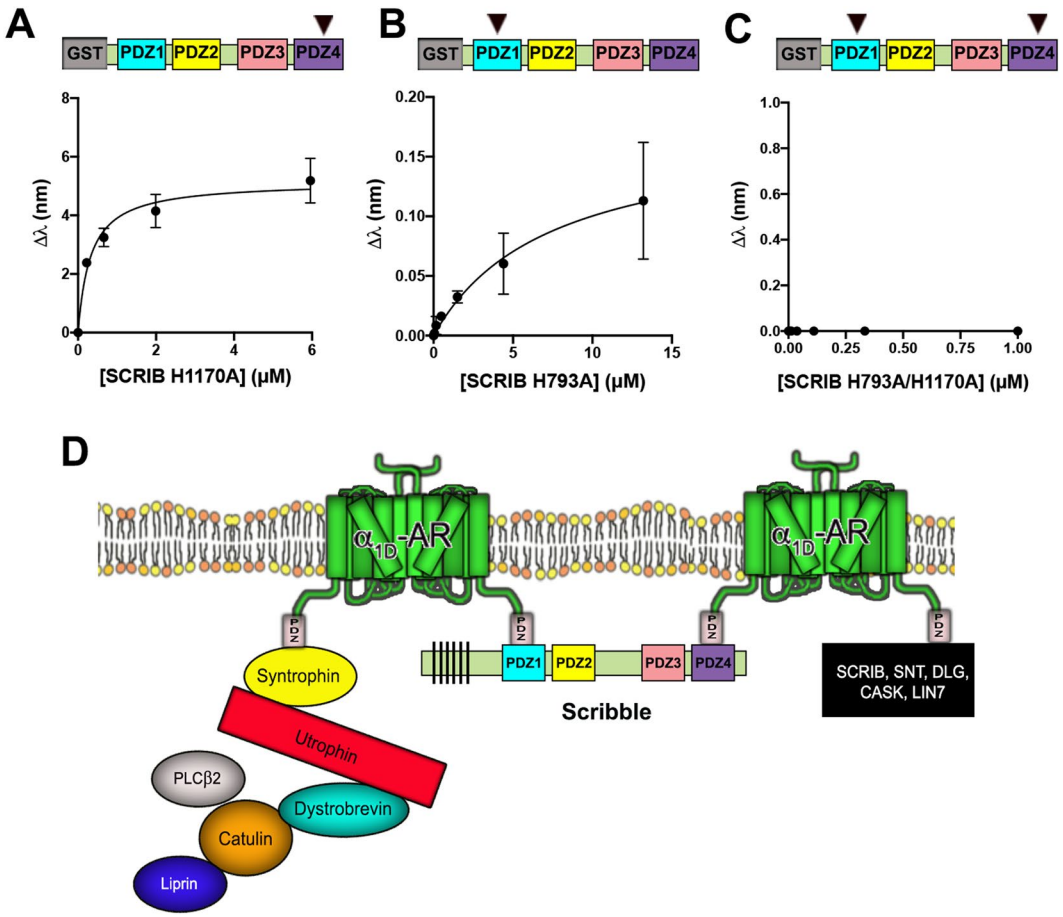


**Figure 6.** Biolayer interferometry analysis of $\alpha_{1D}$-adrenergic receptor C-terminal PDZ ligand:SCRIB H793A/H1170A interactions. Biolayer interferometry (BLI) was used to quantify $\alpha_{1D}$-CT binding to full length SCRIB containing point mutations H1170A (**A**), H793A (**B**), or both H793A and H1170A (**C**). ▼ indicate the SCRIB PDZ domain harboring the denoted H → A mutation. Data are presented as mean ± SEM, n = 3. (**D**) Hypothetical model of the $\alpha_{1D}$-AR:SCRIB:DAPC macromolecular complex in human cells.

**Cell culture.** Human embryonic kidney (HEK) 293 cells were grown in Dulbecco's modified Eagle's medium (DMEM) supplemented with 10% fetal bovine serum and 2 mM L-glutamine. Cells were transfected with 1 mg/ml polyethyleneimine (PEI) and used ~48 h post-transfection. For the development of the SNAP-$\alpha_{1D}$-AR stable cell line, G418 was added to the media 24 h post-transfection. [$^3$H]-Prazosin saturation radioligand binding (data not shown) and PAGE NIR (described in 57) were used to verify SNAP-$\alpha_{1D}$-AR protein expression.

**Label-free DMR assays.** DMR assays were performed in 384 well Corning Epic sensor microplates (Corning, Corning, NY) using the protocol described previously[57]. Data were analyzed with GraphPad Prism software (La Jolla, CA).

**Recombinant protein expression and purification.** Recombinant proteins were expressed in Rosetta™ (DE3) competent cells (EMD Millipore, Burlington, MA) in Miller LB supplemented with 100 μg/mL Ampicillin and 34 μg/mL Chloramphenicol at 37 °C until an $OD_{600} = 0.6–1.0$ was reached; followed by induction with IPTG (1 mM) at 18 °C for 18 h. Cells were harvested by centrifugation and lysed (20 mM Tris-HCl pH 8.0, 200 mM NaCl, 5 mM DTT, Protease inhibitors). GST-tagged protein was immobilized on Pierce® glutathione agarose beads (Thermo Scientific, Waltham, MA) and washed (20 mM Tris-HCl pH 8.0 and 200 mM NaCl). Bound protein was eluted from the beads in wash buffer supplemented with 10 mM glutathione and concentration was determined using Bradford assay. Immobilized protein for crystallography was incubated with TEV at 4 °C for 18 h and subjected to size exclusion chromatography using a Superdex 75 Increase 10/300 GL (GE Healthcare, Chicago, IL) on an AKTA FPLC (GE Healthcare, Chicago, IL) in lysis buffer. The peak 215 nm fractions were collected. SDS-PAGE analysis was employed to determine purity, and protein was flash frozen and stored at −80 °C until needed.

**SNAP GST-pulldown assay.** SNAP-$\alpha_{1D}$-C terminal domain (SNAP-$\alpha_{1D}$-CT) was created by subcloning cDNA encoding the distal 16 amino acids of the human $\alpha_{1D}$-C terminal domain into the 3′ MCS of pSNAP. SNAP and SNAP-$\alpha_{1D}$-CT were then subcloned into a modified pGEX vector to add N-terminal GST tags, expressed in, and purified from *E. coli* using the previously described method (Fig. 4B). Following TEV cleavage and ion

exchange chromatography, SNAP-$\alpha_{1D}$-CT was reacted with BG-782 (1 μM) for 30 min @37 °C in the dark. Serial dilutions of BG-782:SNAP-$\alpha_{1D}$-CT were subjected to SDS-PAGE and near infrared fluorescence (NIR: $\lambda = 800$ nm) was quantified with the LI-COR Odyssey CLx (Fig. 4C; LI-COR, Lincoln, NE). Fluorescence intensity standard curves for SNAP-$\alpha_{1D}$-CT were generated to calculate protein concentrations (Fig. 4D). For GST-pulldown, 25 μL of 1 μM GST-tagged SCRIB proteins and 25 μL of BG-782:SNAP-$\alpha_{1D}$-CT were incubated with 25 μL of packed Pierce® glutathione agarose beads and rotated in the dark for 1 h at 4 °C. Samples were centrifuged @ 500 RPM at 4 °C for 5 min. Supernatant was discarded and beads were washed 3x (20 mM Tris-HCl pH 8.0, 200 mM NaCl, and 0.05% NP-40). Samples were boiled in SDS-sample buffer, and 10 μL aliquots were subjected to PAGE NIR.

**Affinity purification/Co-immunoprecipitation.** TAP purification was performed using the protocol described previously[19,20]. 5 μL of 25 μM BG-782 was included in the 1st overnight solubilization step with 0.5% digitonin to label SNAP-$\alpha_{1D}$-ARs. PAGE NIR was used to observe SNAP-$\alpha_{1D}$-AR protein levels. Gels were then transferred to nitrocellulose and blotted for anti-HA (#2367, Cell Signaling Technology, Danvers, MA) or anti-MYC (#9B11, Cell Signaling Technology, Danvers, MA), then anti-mouse Alexa-Fluor 2° antibodies in the 700–800 nm range (Invitrogen, Carlsbad, CA). Gels and blots were imaged with the LI-COR Odyssey CLx.

**Biolayer interferometry (BLI).** BLI was performed using the Octet Red 96 system (Pall Forte Bio, Fremont, CA). All steps were performed in 20 mM Tris-HCl pH 8.0, 200 mM NaCl, and 0.1% bovine serum albumin. 50 nM of biotin labeled peptide containing the last 20 amino acids of the $\alpha_{1D}$-CT (BioMatik, Cambridge, ON) was immobilized to streptavidin coated probes, followed by biocytin. The immobilized peptide was incubated in serial dilutions of target proteins until steady-state binding was reached. Biocytin was used to determine non-specific binding. For reverse BLI, GST-SCRIB was immobilized using anti-GST probes, and then incubated in serial dilutions of biotin labeled $\alpha_{1D}$-CT.

**Cell surface assay.** HEK293 cell surface expression of SNAP-$\alpha_{1D}$-AR was quantified with cell impermeable SNAP-substrate BG-782 using the method described previously[57]. TO-PRO-3 nuclear stain was used to normalize samples according to cell number. Data were analyzed with GraphPad Prism software.

**X-ray crystallography.** SCRIB PDZ4 R1110G was concentrated to 11 mg/mL in 20 mM Tris at pH 8.0, 200 mM NaCl, and 5 mM DTT and screened against crystallization conditions using a Mosquito Liquid Handler (TTP Labtech, Cambridge, MA). Final crystals were obtained in 21% PEG 3,350 and 0.25 M Ammonium Nitrate. Crystals were flash frozen in mother liquor supplemented with 15% glycerol. All diffraction data was collected at the Advanced Light Source at Berkeley on beam line 8.2.1, integrated with XDS[58], and scaled with AIMLESS[59,60]. Phases were determined by molecular replacement using *Phaser*[61] and SCRIB PDZ4 (39; PDB ID: 4WYT) as a search model. The *Phaser* solution was manually rebuilt over multiple cycles using Coot[62] and refined using *PHENIX*[63]. All images were generated using the PyMOL Molecular Graphics System, Version 1.74 Schrödinger, LLC. Coordinate files have been deposited in the Protein Data Bank under the accession code 6EEY.

**Molecular docking.** The distal 6 amino acids of the $\alpha_{1D}$-AR C-terminus, LRETDI, was modeled into the canonical βB and αB binding pocket of Scribble PDZ4[39] using PyMOL and submitted to FlexPepDock server[50,51]. Models with scores greater than −131 were analyzed for hydrogen bonding (1.5–2.5Å) between peptide and PDZ4. Only interactions identified in greater than 5 models are reported.

## References


1. Overington, J. P., Al-Lazikani, B. & Hopkins, A. L. How many drug targets are there? *Nat. Rev. Drug Discov.* **5**, 993–996 (2006).
2. Shukla, A. K., Xiao, K. & Lefkowitz, R. J. Emerging paradigms of β-arrestin-dependent seven transmembrane receptor signaling. *Trends Biochem. Sci.* **36**, 457–469 (2011).
3. Romero, G., von Zastrow, M. & Friedman, P. A. Role of PDZ proteins in regulating trafficking, signaling, and function of GPCRs: means, motif, and opportunity. *Adv. Pharmacol.* **62**, 279–314 (2011).
4. Ritter, S. L. & Hall, R. A. Fine-tuning of GPCR activity by receptor-interacting proteins. *Nat. Rev. Mol. Cell Biol.* **10**, 819–830 (2009).
5. Tsunoda, S. *et al*. A multivalent PDZ-domain protein assembles signaling complexes in a G-protein-coupled cascade. *Nature* **388**, 243–249 (1997).
6. Hall, R. A. *et al*. The β2-adrenergic receptor interacts with the Na+/H+-exchanger regulatory factor to control Na+/H+ exchange. *Nature* **392**, 626–630 (1998).
7. Lauffer, B. E. *et al*. SNX27 mediates PDZ-directed sorting from endosomes to the plasma membrane. *J. Cell. Biol.* **190**, 565–574 (2010).
8. Gage, R. M., Matveeva, E. A., Whiteheart, S. W. & von Zastrow, M. Type I PDZ ligands are sufficient to promote rapid recycling of G protein-coupled receptors independent of binding to N-ethylmaleimide-sensitive factor. *J. Biol. Chem.* **280**, 3305–3313 (2005).
9. Xu, J. *et al*. β1-adrenergic receptor association with the synaptic scaffolding protein membrane-associated guanylate kinase inverted-2 (MAGI-2). *J. Biol. Chem.* **276**, 41310–41317 (2001).
10. Guillaume, J. L. *et al*. The PDZ protein mupp1 promotes Gi coupling and signaling of the Mt1 melatonin receptor. *J. Biol. Chem.* **283**, 16762–16771 (2008).
11. Dunn, H. A. & Ferguson, S. S. PDZ protein regulation of G protein-coupled receptor trafficking and signaling pathways. *Mol. Pharmacol.* **88**, 624–639 (2015).
12. Carey, L. M. *et al*. Small molecular inhibitors of PSD95-nNOS protein-protein interactions suppress formalin-evoked Fos protein expression and nociceptive behavior in rats. *Neuroscience.* **349**, 303–317 (2017).
13. Lee, W. H. *et al*. ZLcOO2, a putative small-molecule inhibitor of nNOS interaction with NOS1AP, suppresses inflammatory nociception and chemotherapy-induced neuropathic pain and synergizes with paclitaxel to reduce tumor cell viability. *Mol. Pain.* **14**, 1–17 (2018).
14. Lee, W. H. *et al*. Disruption of nNOS-NOS1AP protein-protein interactions suppresses neuropathic pain in mice. *Pain.* **159**, 849–863 (2018).
15. Li, L. L. *et al*. The nNOS-p38 MAPK pathway is mediated by NOS1AP during neuronal death. *J. Neurosci.* **33**, 8185–8201 (2013).
16. Chen, Z., Hague, C., Hall, R. A. & Minneman, K. P. Syntrophins regulate $\alpha_{1D}$-adrenergic receptors through a PDZ domain-mediated interaction. *J. Biol. Chem.* **281**, 12414–12420 (2006).

17. Lyssand, J. S. *et al.* α-Dystrobrevin-1 recruits α-catulin to the $\alpha_{1D}$-adrenergic receptor/dystrophin-associated protein complex signalosome. *Proc. Natl. Acad. Sci. USA* **107**, 21854–21859 (2010).
18. Lyssand, J. S., Lee, K. S., DeFino, M., Adams, M. E. & Hague, C. Syntrophin isoforms play specific functional roles in the $\alpha_{1D}$-adrenergic receptor/DAPC signalosome. *Biochem. Biophys. Res. Commun.* **412**, 596–601 (2011).
19. Camp, N. D. *et al.* Individual protomers of a G protein-coupled receptor dimer integrate distinct functional modules. *Cell Discov.* **1**, 15011, https://doi.org/10.1038/celldisc.2015.11 (2015).
20. Camp, N. D. *et al.* Dynamic mass redistribution reveals diverging importance of PDZ-ligands for G protein-coupled receptor pharmacodynamics. *Pharmacol. Res.* **105**, 13–21 (2016).
21. Garcia-Cazarin, M. L. *et al.* The $\alpha_{1D}$-adrenergic receptor is expressed intracellularly and coupled to increases in intracellular calcium and reactive oxygen species in human aortic smooth muscle cells. *J. Mol. Signal* **3**, 6, https://doi.org/10.1186/1750-2187-3-6 (2008).
22. Petrovska, R., Kapa, I., Klovins, J., Schiöth, H. B. & Uhlén, S. Addition of a signal peptide sequence to the $\alpha_{1D}$-adrenoceptor gene increases the density of receptors, as determined by [$^3$H]-prazosin binding in the membrane. *Br. J. Pharmacol.* **144**, 651–659 (2005).
23. Hague, C., Uberti, M. A., Chen, Z., Hall, R. A. & Minneman, K. P. Cell surface expression of $\alpha_{1D}$-adrenergic receptors is controlled by heterodimerization with $\alpha_{1B}$-adrenergic receptors. *J. Biol. Chem.* **279**, 15541–15549 (2004).
24. Sever, P. S. Alpha 1-blockers in hypertension. *Curr. Med. Res. Opin.* **15**(2), 95–103 (1999).
25. Walden, P. D., Gerardi, C. & Lepor, H. Localization and expression of the $\alpha_{1A}$, $\alpha_{1B}$ and $\alpha_{1D}$-adrenoceptors in hyperplastic and non-hyperplastic human prostate. *J. Urol.* **161**, 635–640 (1999).
26. Hampel, C. *et al.* Modulation of bladder $\alpha_1$-adrenergic receptor subtype expression by bladder outlet obstruction. *J. Urol.* **167**, 1513–1521 (2002).
27. Liu, J. *et al.* The association of DNA methylation and brain volume in healthy individuals and schizophrenia patients. *Schizophr. Res.* **169**, 447–452 (2015).
28. Raskind, M. A. *et al.* Trial of prazosin for post-traumatic stress disorder in military veterans. *N. Engl. J. Med.* **378**, 507–517 (2018).
29. Olson, V. G. *et al.* The role of norepinephrine in differential response to stress in an animal model of posttraumatic stress disorder. *Biol. Psychiatry* **70**, 441–448 (2011).
30. Miller, J. L. Doxazosin dropped from ALLHAT study. *Am. J. Health Syst. Pharm.* **57**, 718 (2011).
31. Stucke, V. M., Timmerman, E., Vandekerckhove, J., Gevaert, K. & Hall, A. The MAGUK protein MPP7 binds to the polarity protein hDlg1 and facilitates epithelial tight junction formation. *Mol. Biol. Cell* **18**, 1744–1755 (2007).
32. Stephens, R. *et al.* The Scribble cell polarity module in the regulation of cell signaling in tissue development and tumorigenesis. *J. Mol. Biol.* **430**, 3585–3612 (2018).
33. Mathew, D. *et al.* Recruitment of scribble to the synaptic scaffolding complex requires GUK-holder, a novel Dlg binding protein. *Curr. Biol.* **12**, 531–539 (2002).
34. Zhu, J. Phosphorylation-dependent interaction between tumor suppressors Dlg and Lgl. *Cell Res.* **24**, 451–463 (2014).
35. Kallay, L. M., McNickle, A., Brennwald, P. J., Hubbard, A. L. & Braiterman, L. T. Scribble associates with two polarity proteins, Lgl2 and Vangl2, via distinct molecular domains. *J. Cell. Biochem.* **99**, 647–664 (2006).
36. Butz, S., Okamoto, M. & Südhof, T. C. A tripartite protein complex with the potential to couple synaptic vesicle exocytosis to cell adhesion in brain. *Cell* **94**, 773–782 (1998).
37. Borg, J. P. *et al.* Identification of an evolutionarily conserved heterotrimeric protein complex involved in protein targeting. *J. Biol. Chem.* **273**, 3163–31636 (1998).
38. Lee, S., Fa, S., Makarova, O., Straight, S. & Margolis, B. A novel and conserved protein-protein interaction domain of mammalian Lin-2/CASK binds and recruits SAP97 to the lateral surface of epithelia. *Mole. Cell. Biol.* **22**, 1778–1791 (2002).
39. Ren, J. *et al.* Interdomain interface-mediated target recognition by the Scribble PDZ34 supramodule. *Biochem. J.* **468**, 133–144 (2015).
40. Long, J. F. *et al.* Supramodular structure and synergistic target binding of the N-terminal tandem PDZ domains of PSD-95. *J. Mol. Biol.* **327**, 203–214 (2003).
41. Grootjans, J. J., Reekmans, G., Ceulemans, H. & David, G. Syntenin-syndecan binding requires syndecan-synteny and the co-operation of both PDZ domains of syntenin. *J. Boil. Chem.* **275**, 19933–19941 (2000).
42. Grembecka, J. *et al.* The binding of the PDZ tandem of syntenin to target proteins. *Biochem. J.* **45**, 3674–3683 (2006).
43. Dicks, M. *et al.* The binding affinity of PTPN13's tandem PDZ2/3 domain is allosterically modulated. *BMC Mol. Cell. Biol.* **20**, https://doi.org/10.1186/s12860-019-0203-6 (2019).
44. Richier, L. *et al.* NOS1AP associates with Scribble and regulates dendritic spine development. *J. Neurosci.* **30**, 4796–4805 (2010).
45. Takizawa, S. *et al.* Human scribble, a novel tumor suppressor identified as a target of high-risk HPV E6 for ubiquitin-mediated degradation, interacts with adenomatous polyposis coli. *Genes Cells.* **11**, 453–464 (2006).
46. Zheng, W. *et al.* An interaction between Scribble and the NADPH oxidase complex controls M1 macrophage polarization and function. *Nat. Cell Biol.* **18**, 1244–1252 (2016).
47. Piguel, N. H. *et al.* Scribble1/AP2 complex coordinates NMDA receptor endocytic recycling. *Cell Rep.* **9**, 712–727 (2014).
48. Hendrick, J. *et al.* The polarity protein Scribble positions DLC3 at adherens junctions to regulate Rho signaling. *J Cell Sci.* **19**, 3583–3596 (2016).
49. Lyssand, J. S. *et al.* Blood pressure is regulated by an $\alpha_{1D}$-adrenergic receptor/dystrophin signalosome. *J. Biol. Chem.* **283**, 18792–18800 (2008).
50. Raveh, B., London, N. & Schueler-Furman, O. Sub-angstrom modeling of complexes between flexible peptides and globular proteins. *Proteins* **78**, 2029–2040 (2010).
51. London, N., Raveh, B., Cohen, E., Fathi, G. & Schueler-Furman, O. Rosetta FlexPepDock web server—high resolution modeling of peptide–protein interactions. *Nucleic Acids Res.* **39**, W249–W253 (2011).
52. Doyle, D. A. *et al.* Crystal structures of a complexed and peptide-free membrane protein–binding domain: molecular basis of peptide recognition by PDZ. *Cell* **85**, 1067–1076 (1996).
53. Mamonova, T. *et al.* Origins of PDZ binding specificity. A computational and experimental study using NHERF1 and the parathyroid hormone receptor. *Biochemistry* **56**, 2584–2593 (2017).
54. Songyang, Z. *et al.* Recognition of unique carboxyl-terminal motifs by distinct PDZ domains. *Science* **275**, 73–77 (1997).
55. Babault, N. *et al.* Peptides targeting the PDZ domain of PTPN4 are efficient inducers of glioblastoma cell death. *Structure* **19**, 1518–1524 (2011).
56. Strickler, N. L. *et al.* PDZ domain of neuronal nitric oxide synthase recognizes novel C-terminal peptide sequences. *Nat. Biotechnol.* **15**, 336–342 (1997).
57. Kountz, T. S. *et al.* Endogenous N-terminal domain cleavage modulates $\alpha_{1D}$-adrenergic receptor pharmacodynamics. *J. Biol. Chem.* **291**, 8210–18221 (2016).
58. Kabsch, W. XDS. *Acta Crystallogr. D Biol. Crystallogr.* **66**, 125–132 (2010).
59. Evans, P. Scaling and assessment of data quality. *Acta. Crystallogr. D Biol. Crystallogr.* **62**, 72–82 (2006).
60. Winn, M. D. *et al.* Overview of the CCP4 suite and current developments. *Acta. Crystallogr. D Biol. Crystallogr.* **67**, 235–242 (2011).
61. McCoy, A.J. *et al.* Phaser crystallographic software. *J. Appl. Crystallogr.* **40**, 658–674.
62. Emsley, P. & Cowtan, K. (2004) Coot: model-building tools for molecular graphics. *Acta. Crystallogr. D Biol. Crystallogr.* **60**, 2126–2132 (2007).
63. Adams, P. D. *et al.* PHENIX: a comprehensive Python-based system for macromolecular structure solution. *Acta. Crystallogr. D Biol. Crystallogr.* 66, (213–221 (2010).

## Acknowledgements
This research was funded by NIGMS T32GM007750 (E.J., D.A.H.) and R01GM100893 (C.H.) and Howard Hughes Medical Institute (N.Z.).

## Author Contributions
E.M.J. and C.H. designed and performed experiments and wrote the manuscript. D.A.H., D.D. and A.S. performed experiments. T.R.H. contributed to experimental design and analysis of BLI experiments. E.M.J., P.L.H. and N.Z. contributed to collection and interpretation of X-ray crystallography data. All co-authors contributed to editing and reviewing the manuscript.

## Additional Information
**Supplementary information** accompanies this paper at https://doi.org/10.1038/s41598-019-50671-6.

**Competing Interests:** The authors declare no competing interests.

**Publisher's note** Springer Nature remains neutral with regard to jurisdictional claims in published maps and institutional affiliations.